# Experimental investigation on residual reflectance of Nd:glass amplifier edge cladding

**Junjiang Hu (胡俊江)*, Liyan Zhang (张丽艳), Jiachuan Ni (倪加川), Tao Meng (孟 涛), Lei Wen (温 磊), Youkuo Chen (陈尤阔), Jingping Tang (唐景平), Biao Wang (王 标), Shubin Chen (陈树彬), Wei Chen (陈 伟), and Lili Hu (胡丽丽)**

*Shanghai Institute of Optics and Fine Mechanics, Chinese Academy of Sciences, Shanghai 201800, China*
**Corresponding author: hjj@siom.ac.cn*

Received April 2, 2020; accepted May 15, 2020; posted online July 21, 2020

A novel four light ray path test method for measuring residual reflectance has been presented. Residual reflectance spatial distribution at a cladding interface was measured using the technique. Residual reflectance could be on the order of $10^{-5}$ by matching the refractive index of Nd:glass, polymer, and cladding glass and eliminating defects in the adhesive layer. Residual reflection spatial distribution appears to be similar to Newton rings due to the edge surface flatness. The relationship between the residual reflectance and the edge surface flatness was discussed, and the results revealed that the edge surface flatness is very important during the cladding process.

*Keywords: residual reflectance; edge cladding; Nd:glass amplifier.*
*doi: 10.3788/COL202018.091402.*

The large-size $Nd^{3+}$-doped phosphate glass (Nd:glass) disk is the most used and the largest optical element in high-peak power solid state laser systems such as SG-II, SG-III in China, LMJ in France, and NIF in America for inertial confinement fusion (ICF) research[1–7]. The Nd:glass disk is also used as the working material of the pump lasers in optical parametric chirped-pulse amplification (OPCPA) systems[8]. The extraction efficiency of the stored energy of the laser glass disks is affected by amplified spontaneous emission (ASE) and parasitic oscillation (PO), which will consume the inverted population in the Nd:glass gain medium, and the effects of ASE and PO were detailed in Refs. [9,10]. So, in order to minimize the loss of stored energy in the laser glass amplifiers, the edges of the amplifier were ground and polished with a slight tilt. Tilting strategy can reduce the reflection threat from small bond delamination near the disk face and can also reduce the index match accuracy required to suppress the surface PO. The flat cladding glass strips ($Cu^{2+}$-doped phosphate absorbing glass) were adhesively bonded to these edges using a composite polymer, and the edge cladding process was detailed as described in Refs. [11–14]. The absorbing glass absorbs the reflected or scattered ASE photons and suppresses parasitic oscillations at the laser wavelength. Further, the energy consumption by the ASE and PO photons can be decreased significantly. The absorption efficiency and parasitic threshold are decided by the residual reflectance at the interface of laser glass, polymer, and cladding glass. The parasitic threshold condition for the bulk mode and surface mode has been demonstrated by Glaze *et al.*[9]. It is a function of the residual reflectance as defined by

$$R_s e^{n\bar{\alpha}D} = 1 \quad \text{(bulk mode)}, \tag{1}$$

$$R_r e^{\alpha_s D} = 1 \quad \text{(surface mode)}, \tag{2}$$

where $R_r$ is the residual reflectance, $n$ is the refractive index of the laser glass, $\bar{\alpha}$ is the average gain coefficient, $\alpha_s$ is the surface gain coefficient, and $D$ is the length of the disk major axis. It shows that lower residual reflectance can provide a higher threshold, which can prevent parasitic oscillation and increase the gain of the amplifiers.

The primary reflection sources from the edge coated directly with an absorbing substance have been detailed by Hirota and Izumitani[15]. When the polymer cladding techniques were used, the residual reflectance was likely to be determined by the following factors: (1) refractive index mismatch of the laser glass, polymer, and cladding glass; (2) defects such as bubbles, scratches, and delamination in the cladding layer; (3) absorption and optical quality of the cladding glass; (4) reflection from the outside surface of the cladding glass strips; (5) subsurface defects in the edge cladding surface; (6) flatness of the bonding surface, and so on. Influences of the refractive index mismatching, the defects in the cladding layer, the absorption and quality of the absorbing glass, as well as the reflection from the outside surfaces on the residual reflection were exhibited in Refs. [14,15]. The influence of subsurface defects in the edge cladding surface was also discussed in Ref. [16]. In this Letter, the residual reflectance of the large-scale sample was measured accurately, and the influence of the edge surface flatness was discussed for the first time.

It is more difficult to measure the residual reflectance at the edge cladding interface in the actual used amplifier. First, the edge cladding interface was inside the amplifier after the edge cladding process finished. Therefore, it is difficult to measure the residual reflectance directly. At the same time, it is difficult to eliminate the influence of the absorption and surface reflection of the amplifier. Second, the refractive indices of the Nd:glass, polymer,

 

and cladding glass were in good matching within ±0.003. This accuracy matching makes the order of magnitude of the residual reflectance much less than $10^{-3}$. Hirota and Izumitani used a 587.6 nm light source to test the residual reflectance of the edge interface[15]. This method could only be used for single point testing, which is not suitable for large samples. Bo *et al.* measured the residual reflectance of the edge interface with a spectrophotometer[17]. But the influence of the sample surface reflectance and absorption can only be deducted by calculation, and the approach is also unable to test large-scale samples.

In this Letter, we established a novel four light ray path test method that was based on a fiber technique. This method can detect the reflection photons from the adhesive surface directly off large-scale samples with high sensitivity and satisfied precision requirements. It can perform millimeter-size spatial resolution at the same time. This test method is schematically illustrated in Fig. 1. A 1064 nm laser was used as the test light source, and a 633 nm laser was used as the indicator light source for the optical path adjusting through the beam splitter (BS). An attenuator was used to tune the power of the laser beam. A lens was used for the laser beam focusing. The residual reflectance signal is very weak, typically on the order of $10^{-3}$ to $10^{-5}$. In order to reduce the impact of noise and detect weak photoelectric signals, a lock-in amplifier and an optical chopper were used in the experiment device. The laser was modulated at a specific frequency by the chopper, and the frequency was sent to the lock-in amplifier as a reference signal. The $1 \times 4$ optical coupler/splitter ($1 \times 4$ OC) was used to couple the laser beam into optical fiber and to divide the laser light into four beams. The optical collimator system (C1, C2, C3, and C4) includes an optical fiber collimator (OFC), an optical mechanical switch (OMS), and an attenuator (ATR). This system transferred the four beams ($I_1$, $I_2$, $I_3$, and $I_4$) to the reference sample (RF), the edge cladding interface, the neodymium glass sample, and the air, respectively. Then the four lights were collected by a 4-port integrating sphere (4-port IS). One port of the integrating sphere was equipped with Si photodiode detector. The first beam $I_1$ was used to calibrate the measurement result of the residual reflectance. The second beam $I_2$ was used to irradiate the edge cladding interface. The third beam $I_3$ was used to traverse the light through the sample in order to eliminate the reflection and absorption influence of the sample, and the fourth beam $I_4$ was used to inspect the power stability of the laser source. Four optical mechanical switches were applied to select one of the four lights at a certain frequency. This method can use the same detector to improve the measurement accuracy. The large sample was placed on a motorized translation stage. Intensities of the four lights were measured by the same photoelectric detector separately.

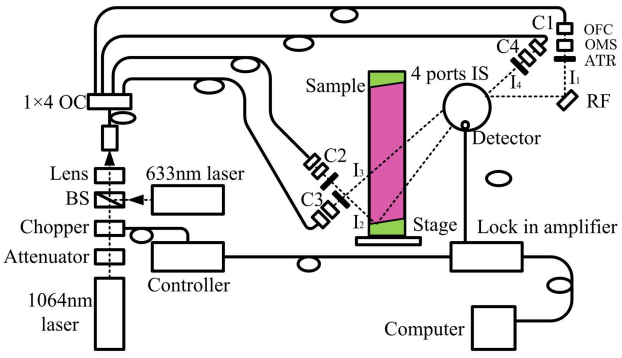


Fig. 1. Schematic diagram of the experimental setup.

Figure 2 is a schematic illustration of ray geometry at the edge cladding interface. $I_1$ and $I_4$ are the intensity of calibration and inspection light, respectively. $I_2$ and $I_3$ are the intensity of the second and third parts. The residual reflectance $R_r$ could be calculated as

$$R_r = \frac{I'_3}{I'_2} \cdot \frac{I_2}{I_3} \cdot \frac{(1-R_2)}{(1-R_3)} \cdot e^{-\alpha[L_2-(L_{31}+L_{32})]} \cdot \frac{(1-R'_2)}{(1-R'_3)}, \tag{3}$$

in which $\alpha$ is the absorption coefficient of Nd:glass; $R_2$, $R_3$, $R'_2$, and $R'_3$ are the surface reflectivity; and $L_2$, $L_{31}$, and $L_{32}$ are the geometric length of the light passing through the sample. The angles of incidence of the second and the third light are equal (about 45 deg), and the slit angle $\theta$ of the edge is quite small (about 2 deg). The absorption coefficient $\alpha$ is much less than 0.0015 $\text{cm}^{-1}$. Then it can be derived that $R_2 = R_3$, $R'_2 \approx R'_3$, $\alpha L_2 \approx \alpha(L_{31} + L_{32})$. The residual reflectance is obtained as simple as follows:

$$R_r = \frac{I'_3}{I'_2} \cdot \frac{I_2}{I_3}. \tag{4}$$

Obviously, the only thing that needs to be measured is the intensity of the second and the third beams before and after the sample is placed. In the experiment, $I_2 = C_{24} I_4$, and $I_3 = C_{34} I_4$. $C_{24}$ and $C_{34}$ are the beam splitting ratios

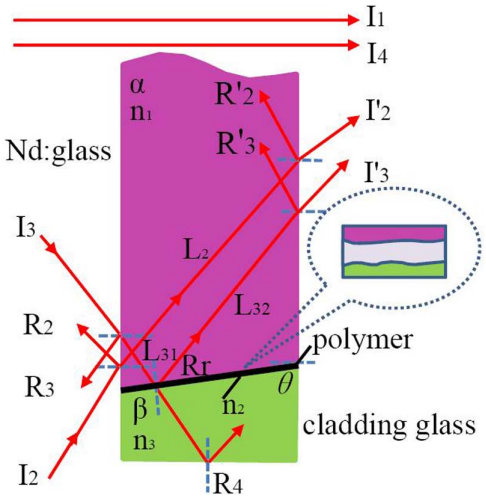


Fig. 2. Schematic illustration of the ray geometry at the edge of the cladding interface.

and can be regarded as constants. Therefore, $I_2$ and $I_3$ can be obtained by $I_4$.

A 400 mm × 400 mm × 43 mm Nd:glass sample was prepared. The edges of the Nd:glass were ground and polished with a tilt of about 2 deg. The 420 mm × 43 mm × 17 mm cladding glass strips were also ground and polished and then bonded to these Nd:glass edges with a polymer[18]. The structure of the cladding interface is also shown in Fig. 2. $\beta$ is the absorption coefficient of the cladding glass. In the experiment, the value of $\beta$ is approximately 2.8 $cm^{-1}$, and the cladding glass thickness is about 1.2 cm. $n_1, n_2$, and $n_3$ are the refractive indices of the Nd:glass, the polymer, and cladding glass, respectively, and usually they will match well within ±0.003[19]. The refractive index was tested by the prism coupling method[20]. The measured $n_1, n_2$, and $n_3$ values are 1.5306, 1.5312, and 1.5336, respectively, at 1064 nm. This represents a precise refractive-index matching at the cladding interface. Before bonding, the edge surface flatness was measured with a Zygo Fizeau interferometer. After the bonding was completed, the large surfaces of the sample were ground and polished. The adhesive layer thickness was then measured by an optical microscope. After that, the residual reflectance test was carried out on the residual reflection test equipment.

The edge surface flatness of the Nd:glass is about 5.4 μm peak-to-valley (PV), and that of the cladding glass is about 7.0 μm PV. The adhesive layer thickness is approximately 5–10 μm.

The residual reflectance $R_r$ is shown in Fig. 3. The maximum value of $R_r$ is about $5.8 \times 10^{-5}$, while the minimum value is about $0.9 \times 10^{-5}$, and the mean value is about $3.3 \times 10^{-5}$. Note that under the condition of matched refractive index, matched and eliminated defects in the adhesive layer $R_r$ is quite low. At the same time, the deviation of $R_r$ can be observed in different positions even under the same bonding conditions, as shown in Fig. 4. It can also be seen that the $R_r$ spatial distribution appears to be similar to Newton rings. The reason is that the coherent length of the test laser wavelength is far greater than the adhesive layer thickness, which is mainly affected by the edge surface flatness between the Nd:glass and cladding glass. The reflections from the two boundaries (Nd:glass-polymer and polymer-cladding glass) can add either phase coherence or phase incoherence, thus forming the interference fringes[13].

In the longitudinal direction of the length of the bonding interface, the edge surface flatness PV in the middle region of the Nd:glass and cladding glass is about 3.4 μm and 6.4 μm, respectively. The residual reflectance varies

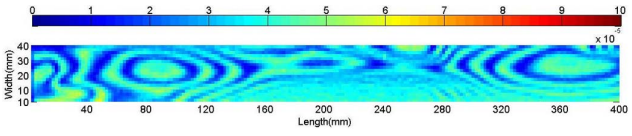


Fig. 3. Distribution of the reflectance at the interface.

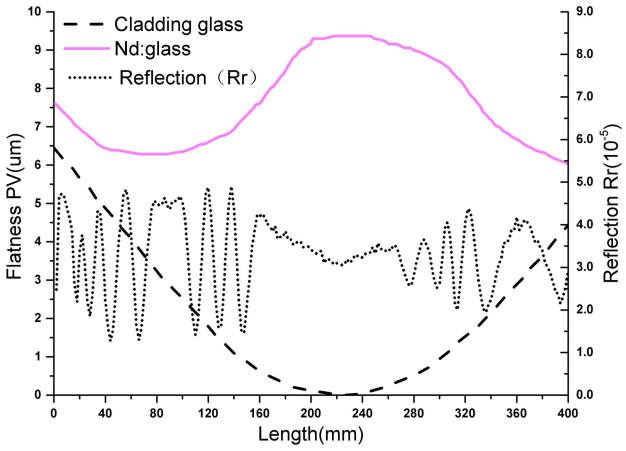


Fig. 4. Relationship between the flatness and reflectance in the center region.

from $1.3 \times 10^{-5}$ to $4.9 \times 10^{-5}$. Its fluctuation is shown in Fig. 4. Clearly, the larger the edge surface flatness gradient causes, the greater the residual reflectance fluctuation, and vice versa, which obeys the principle of Newton rings. So, we could infer that the spatial distribution of the residual reflectance was related to the edge cladding surface flatness.

In conclusion, a four optical ray method for testing residual reflectance was presented. It can cleverly eliminate the influence of surface reflection and material absorption, thus improving the accuracy of the test results. The residual reflectance spatial distribution of a large-scale sample at the cladding interface was measured. Results show that the residual reflectance could be on the order of $10^{-5}$ by matching the refractive index of the Nd:glass, polymer, and cladding glass and eliminating the defects in the adhesive layer. Simultaneously, the residual reflection spatial distribution appears to be similar to Newton rings due to the edge cladding surface flatness. Edge surface flatness could affect the residual reflectance. The results revealed that the edge cladding surface flatness was significant in the cladding process. The experimental results could be employed for the cladding process.

The authors wish to thank the Inertial Confinement Fusion Program in China for its research support, and Dr. Zhouling Wu and Dr. Jian Chen of ZC Optoelectronic Technologies Ltd. for discussion and assistance about residual reflectance measurement equipment.

## References

1. Z. Jiang, Chin. J. Lasers **33**, 1265 (2006).
2. L. Hu, S. Chen, J. Tang, B. Wang, T. Meng, W. Chen, L. Wen, J. Hu, S. Li, Y. Xu, Y. Jiang, J. Zhang, and Z. Jiang, High Power Laser Sci. Eng. **2**, e1 (2016).
3. J. H. Campbell, J. S. Hayden, and A. J. Marker, "High-power solid-state lasers from a laser glass perspective," LLNL-JRNL-464385 (2010).
4. S. E. Bodner, A. J. Schmitt, and J. D. Sethian, High Power Laser Sci. Eng. **1**, 2 (2013).

5. X. Deng, Q. Zhu, W. Zheng, X. Wei, F. Jing, D. Hu, W. Zhou, B. Feng, J. Wang, Z. Peng, L. Liu, Y. Chen, L. Ding, D. Lin, L. Guo, and Z. Dang, Proc. SPIE **8786**, 87861G (2013).
6. J. Zhu, J. Zhu, X. Li, B. Zhu, W. Ma, X. Lu, W. Fan, Z. Liu, S. Zhou, G. Xu, G. Zhang, X. Xie, L. Yang, J. Wang, X. Ouyang, L. Wang, D. Li, P. Yang, Q. Fan, M. Sun, C. Liu, D. Liu, Y. Zhang, H. Tao, M. Sun, P. Zhu, B. Wang, Z. Jiao, L. Ren, D. Liu, X. Jiao, H. Huang, and Z. Lin, High Power Laser Sci. Eng. **6**, e55 (2018).
7. J. Guo, J. Wang, H. Wei, W. Huang, T. Huang, G. Xia, W. Fan, and Z. Lin, High Power Laser Sci. Eng. **7**, e8 (2019).
8. J. Bromage, S.-W. Bahk, I. A. Begishev, C. Dorrer, M. J. Guardalben, B. N. Hoffman, J.B. Oliver, R. G. Roides, E. M. Schiesser, M. J. Shoup, M. Spilatro, B. Webb, D. Weiner, and J. D. Zuegel, High Power Laser Sci. Eng. **7**, e4 (2019).
9. J. A. Glaze, S. Guch, and J. B. Trenholme, Appl. Opt. **12**, 33 (1974).
10. J. B. Trenholme, "Fluorescence amplification and parasitic oscillation limitations in disc lasers," NRL Memorandum Report No. 2480 (1972).
11. M. Sawicka, M. Divoky, A. Lucianetti, and T. Mocek, Laser Particle Beams **31**, 553 (2013).
12. J. M. Mcmahon, J. L. Emmett, J. F. Holzrichter, and J. B. Trenholme, IEEE J. Quantum. Electron. **9**, 992 (1973).
13. K. S. Jancaitis, H. T. Powell, J. B. Trenholme, and J. E. Murray, "Composite Polymer/glass edge cladding for Nova replacement disks," Laser Program Annual Report (1985).
14. J. H. Campbell and G. Edwards, in *Proceedings of Laser Induced Damage in Optical Material* (1988), p. 19.
15. S. Hirota and T. Izumitani, Appl. Opt. **18**, 97 (1979).
16. B. Wang, J. Zhang, S. Shi, K. You, and J. Zhu, High Power Laser Sci. Eng. **4**, e9 (2016).
17. T. Bo, H. Liu, Y. Huang, X. Zhang, Y. Zhang, and Y. Wang, Opt. Tech. **38**, 3 (2012).
18. T. Meng, J. Tang, J. Hu, L. Wen, L. Chen, W. Chen, and L. Hu, China Patent ZL20101 0273819.7 (September 6, 2010).
19. H. Powell, M. Riley, and C. R. Wolfe, US Patent 4849036 (July 18, 1989).
20. J. Hu, T. Meng, H. Chen, L. Wen, J. Tang, C. Wang, Y. Lin, S. Chen, W. Chen, and L. Hu, Chin. Opt. Lett. **12**, 101401 (2014).